Published in final edited form as:
Cell. 2012 December 7; 151(6): 1283–1295. doi:10.1016/j.cell.2012.10.041.

TMHS is an Integral Component of the Mechanotransduction Machinery of Cochlear Hair Cells

Wei Xiong[1], **Nicolas Grillet**[1], **Heather M. Elledge**[1], **Thomas F.J. Wagner**[1], **Bo Zhao**[1], **Kenneth R. Johnson**[2], **Piotr Kazmierczak**[1], and **Ulrich Müller**[1,*]

[1]The Dorris Neuroscience Center, Department of Cell Biology, The Scripps Research Institute, 10550 N. Torrey Pines Road, La Jolla, CA 92037, USA

[2]The Jackson Laboratory, Bar Harbor, ME 04609

SUMMARY

Hair cells are mechanosensors for the perception of sound, acceleration and fluid motion. Mechanotransduction channels in hair cells are gated by tip links, which connect the stereocilia of a hair cell in the direction of their mechanical sensitivity. The molecular constituents of the mechanotransduction channels of hair cells are not known. Here we show that mechanotransduction is impaired in mice lacking the tetraspan TMHS. TMHS binds to the tip-link component PCDH15 and regulates tip-link assembly, a process that is disrupted by deafness-causing *Tmhs* mutations. TMHS also regulates transducer channel conductance and is required for fast channel adaptation. TMHS therefore resembles other ion channel regulatory subunits such as the TARPs of AMPA receptors that facilitate channel transport and regulate the properties of pore-forming channel subunits. We conclude that TMHS is an integral component of the hair cells mechanotransduction machinery that functionally couples PCDH15 to the transduction channel.

INTRODUCTION

Our senses of hearing, balance, proprioception and touch rely on the process of mechanoelectrical transduction, the conversion of mechanical force into electrical signals. Despite the importance of mechanotransduction for perception, the molecular mechanisms that control this process are not well understood. Electrophysiological recordings and imaging studies have revealed that in mechanosensory hair cells of the inner ear mechanically gated ion channels are localized close to the tips of stereocilia, actin-rich projections that emanate from the apical cell surface. Sound induced vibrations or motion lead to deflection of the stereociliary bundles, which directly control the activity of the mechanotransduction channels in stereocilia. It is thought that tip links, fine extracellular filaments that connect the tips of neighboring stereocilia, transmit tension force onto the transduction channels (Gillespie and Muller, 2009).

In recent years, significant progress has been made in the identification of components of the mechanotransduction machinery of hair cells (Fig. 1A). These studies have shown that tip

*Corresponding Author The Dorris Neuroscience Center The Scripps Research Institute 10550 N. Torrey Pines Rd La Jolla, CA 92037, USA P: 858-784-7288 F: 858-784-7299 umueller@scripps.edu.

links are formed by CDH23 homodimers that interact with PCDH15 homodimers to form the upper and lower parts of tip links (Ahmed et al., 2006; Kazmierczak et al., 2007; Siemens et al., 2004; Sollner et al., 2004). The adaptor proteins harmonin and SANS, and the motor protein myosin 7a (Myo7a) bind in vitro to each other and to CDH23 (Adato et al., 2005; Bahloul et al., 2010; Boeda et al., 2002; Siemens et al., 2002) and co-localize at the upper insertion site of tip links (Grati and Kachar, 2011; Grillet et al., 2009b), suggesting that they form a protein complex important for transduction. Consistent with this model, Myo7a is implicated in setting resting tension in the transduction machinery (Kros et al., 2002), while harmonin regulates channel activation and adaptation (Grillet et al., 2009b; Michalski et al., 2009). SANS has been proposed to regulate in tip-link assembly (Caberlotto et al., 2011), and Myo1c, which co-immunoprecipitates with CDH23 (Siemens et al., 2004), is implicated in regulating slow adaptation (Holt et al., 2002). Intriguingly, while null mutations in the genes encoding CDH23, PCDH15, harmonin, SANS, and Myo7a disrupt stereociliary bundles and cause deaf-blindness (Usher Syndrome Type 1, USH1), subtle mutations cause less severe forms of the disease (McHugh and Friedman, 2006; Sakaguchi et al., 2009). Subtle mutations in tip-link associated proteins might affect the properties of the hair cells transduction machinery, a model that is supported by the analysis of mice carrying missense mutations in CDH23 and harmonin (Grillet et al., 2009b; Schwander et al., 2009).

Despite this progress, it is not known which genes encode subunits of the mechanotransduction channel of hair cells. Ca^{2+} enters stereocilia upon mechanical stimulation near the lower tip-link insertion site, indicating that transduction channels are present in proximity to PCDH15 (Beurg et al., 2009). Mechanotransduction in mouse hair cells requires the transmembrane channel-like genes TMC1 and TMC2 (Kawashima et al., 2011), but it is unclear whether these proteins are channel subunits. To identify components of the mechanotransduction channel of hair cells, we have systematically screened mutant mouse lines with auditory impairment for defects in their mechanotransduction machinery. Here we describe the phenotypic consequences caused by mutations affecting TMHS (tetraspan membrane protein of hair cell stereocilia), which lead to autosomal recessive non-syndromic hearing loss (DFNB67) in humans (Shabbir et al., 2006), and deafness in *hurry-scurry* mice (Longo-Guess et al., 2005). TMHS is a member of the tetraspan superfamily, which encodes proteins with diverse functions such as tight junction proteins, gap junction proteins, ion-channel subunits, and tetraspanins. However, the function of TMHS in hair cells and the mechanism by which mutations in its gene cause deafness are not known.

Here we show that TMHS is an auxiliary subunit of the hair cells mechanotransduction channel. Ion channels most commonly consist of pore forming subunits and auxiliary subunits. Examples for auxiliary subunits include the γ1-subunit of Ca_v channels and the TARP subunits of AMPA receptors. These auxiliary subunits control transport of the channel complex to the plasma membrane and regulate the gating properties of pore forming channel subunits (Dai et al., 2009; Jackson and Nicoll, 2011; Pongs and Schwarz, 2010; Vacher et al., 2008). Like the γ1-subunit and TARPs, TMHS belongs to the tetraspan family. It binds to PCDH15, controls the assembly of the hair cells mechanotransduction machinery, regulates the properties of their mechanotransduction channels, and is required for adaptation.

RESULTS

Mechanotransduction defects in TMHS-deficient hair cells

Several laboratories including ours have identified spontaneously arising and chemically induced mutant mouse lines with defects in auditory function. To identify the extent to which mechanotransduction is affected in these lines, we measured in many of them

transducer currents in postnatal day (P) 7 outer hair cell (OHCs) using whole cell recordings (Fig. 1B). We included mouse lines generated by gene targeting, such as *harmonin-PDZ2AAA* mice that carry a point mutation in harmonin (Grillet et al., 2009b). Hair bundles were stimulated with a stiff probe. In wild-type mice, excitatory stimuli elicited transducer currents that reached peak currents of 571.9 ± 20 pA (n=9). Peak amplitude of transducer currents was not reduced in some mutant lines such as pejvakin-deficient *sirtaki* mice and CDH23-deficient *salsa* mice, but more severely in others such as whirlin-deficient *rumba* mice, MyoXVa-deficient *pogo* mice, and *harmonin-PDZ2AAA* mice (Fig. 1B). The most striking defect was observed in two lines of TMHS-deficient mice, with ~90% decrease in peak amplitude (Fig. 1B). One of these lines, *hurry-scurry*, carries a point mutation in TMHS (Longo-Guess et al., 2005). The second line, $Tmhs^{tm1kjn}$ (referred to as $Tmhs^{-/-}$) was generated by knocking LacZ into the *Tmhs* locus (Longo-Guess et al., 2007). Subsequent studies were carried out with $Tmhs^{-/-}$ mice, since they contain a *Tmhs*-null allele (Longo-Guess et al., 2007).

TMHS expression in hair cells, and hair bundle morphology in $Tmhs^{-/-}$ mice

It has been reported that TMHS is transiently expressed in developing hair cells, and that $Tmhs^{-/-}$ mice have mild morphological hair bundle defects (Longo-Guess et al., 2007). To extend these findings and to determine the extent to which the mechanotransduction defect in $Tmhs^{-/-}$ hair cells is a secondary consequence of morphological defects, we investigated by in situ hybridization the *Tmhs* expression pattern, and we analyzed hair bundle morphology. TMHS mRNA was expressed in inner hair cells (IHCs) and OHCs of the cochlear as well as in vestibular hair cells (Fig. 1C). Expression levels correlated with maturation of the transduction machinery. At the cochlear apex, which functionally matures after the cochlear base (Waguespack et al., 2007), expression levels were low at P1 and increased thereafter (Fig. 1C). Robust expression was observed in mature hair cells throughout the cochlea at P25, the last time point analyzed (Fig. 1C).

We next evaluate hair bundle morphology by scanning electron microscopy (SEM). To obtain quantitative values, we determined the height difference between the rows of stereocilia (Supplementary Fig. S1). In $Tmhs^{-/-}$ mice, hair bundles at the cochlear base showed mild defects at P3, which manifested as greater variations of the height differences between stereocilia in different rows compared to wild-type. The defects became more pronounced along the length of the cochlear duct at P5 and increased in severity thereafter (Fig. 1D; Supplementary Fig. S1). Morphological hair bundle defects were mild at P5 and P7 when mechanotransduction was strongly affected (Fig. 1B,D). We also observed strong transduction defects at P0 and P4 (data not shown) suggesting that the hair bundle morphological defects alone cannot explain the functional defects.

To further investigate the relationship between hair bundle morphology and function, we analyzed hair bundles in other mutant mouse lines with defects in transduction. We did not observe a clear correlation between the two phenotypes. For example, peak amplitude of transducer currents was reduced by 44% in *rumba* mice and by 60% in *harmonin-PDZ2AAA* mice (Fig. 1B). The former had short stereocilia (Fig. 1D). The latter showed disruptions of the staircase that was similar in magnitude to $Tmhs^{-/-}$ mice (Fig. 1D). These findings suggest that mechanotransduction defects in OHCs from $Tmhs^{-/-}$ mice are likely not explained primarily by the defects in hair bundle morphology.

Tip-link defects in $Tmhs^{-/-}$ mice

We next determined the TMHS expression pattern by immunohistochemistry. Between P4 and P6, TMHS was expressed in stereocilia in a punctate pattern (Fig. 2A). The pattern resembled the distribution of the tip-link components CDH23 and PCDH15, which are at

this age localized throughout the bundle with only some protein at tip links (Lagziel et al., 2005; Michel et al., 2005; Siemens et al., 2004). TMHS staining was also detectable at the tip-link region (Fig. 2A, arrows). HA-tagged TMHS that was expressed in OHCs by electroporation was targeted towards the tips of stereocilia with some of the protein located in the tip-link region (Fig. 2B). After P7, the amount of TMHS detectable by immunostaining drastically decreased. Since TMHS mRNA is robustly expressed in adult hair cells (Fig. 1C), low levels of TMHS protein likely persist but were difficult to detect. Similar observations have been made for other tip-link associated proteins such as CDH23 and harmonin, which are detected in mature hair cells with few antibodies (Boeda et al., 2002; Grillet et al., 2009b; Kazmierczak et al., 2007; Lagziel et al., 2005; Lefevre et al., 2008; Michel et al., 2005; Siemens et al., 2004).

The localization of TMHS towards sterociliary tips suggested that defects in mechanotransduction in *Tmhs*$^{-/-}$ mice might be caused by abnormal tip-link function. We therefore analyzed by SEM the integrity of tip links in hair cells from *Tmhs*$^{-/-}$ mice. At P7, stereocilia from control mice were connected by an array of extracellular filaments as reported (Fig. 2C) (Goodyear et al., 2005). Higher magnification views revealed the presence of tip links in IHCs and OHCs (Fig. 2D). Stereocilia in hair bundles from *Tmhs*$^{-/-}$ mice were also connected by extracellular filaments but tip links were rarely observed (Fig. 2C,D). To quantify tip-link numbers, we focused in P7 hair cells on linkages between the longest rows of stereocilia and their next shorter neighbors. Tip links were at this age more difficult to distinguish from other linkages in the shorter rows of stereocilia. At P7, control IHC (n=17 IHCs) from the medial part of the cochlea contained 2.8 times more tip links compare to *Tmhs*$^{-/-}$ (n=14 IHCs), while OHC from the apical/medial part of the cochlea contained 2.2 times more tip links in controls (n=7 OHCs) compare to mutants (n=7 OHCs) (Fig. 2E).

Interdependence of PCDH15 and TMHS localization

To determine the mechanism by which mutations in TMHS affect tip links, we analyzed the TMHS expression pattern in mice with mutations in CDH23 and PCDH15. Similarly, we evaluated CDH23 and PCDH15 expression in *Tmhs*$^{-/-}$ mice. Stereocilia are splayed in PCDH15- and CDH23-deficient hair bundles (Alagramam et al., 2001; Di Palma et al., 2001; Wilson et al., 2001). At P1, TMHS expression at tips of stereocilia was maintained in the splayed bundles from CDH23-deficient *waltzer*$^{v2J/v2J}$ mice, but expression was drastically reduced in PCDH15-deficient *Ames waltzer*$^{av3J/av3J}$ mice (Fig. 3A). Conversely, CDH23 was expressed at P6 in hair bundles from *Tmhs*$^{-/-}$ hair cells, while PCDH15 expression levels were reduced in the mutants (Fig. 3A). At P0 and P3, residual levels of PCDH15 were present in stereocilia (data not shown), indicating that loss of PCDH15 localization to hair bundles was progressive. These data suggest that TMHS is required for the efficient localization of PCDH15 to hair bundles and vice versa. Perturbations in the formation of tip links in *Tmhs*$^{-/-}$ mice are therefore likely caused, at least in part, by inefficient localization of PCDH15 to stereocilia.

TMHS binds PCDH15

To define whether TMHS affects the distribution of PCDH15 in hair cells directly or indirectly, we next asked whether TMHS and PCDH15 are part of a protein complex. We co-expressed TMHS-HA and PCDH15 in HEK293 cells, focusing on PCDH15-CD1, -CD2, and -CD3, three PCDH15 isoforms that differ in their cytoplasmic domains (Ahmed et al., 2006). TMHS co-immunoprecipitated with all three isoforms (Fig. 3B,C; data not shown), but not with N-cadherin (Fig. 3C), an unrelated cadherin.

The PCDH15-CD1, -CD2, and -CD3 cytoplasmic domains share a conserved membrane proximal (CR) domain followed by isoform specific N-terminal domains (Ahmed et al., 2006). TMHS co-precipitated with a PCDH15 mutation truncated immediately at the C-terminus of the CR domain (Fig. 3C), and with a PCDH15 fragment consisting of the CR and CD3 domains, but not with a fragment consisting of the CD3-specific domain only (Fig. 3C). Finally, TMHS co-immunoprecipitated with a chimeric protein, where the N-cadherin transmembrane domain was substituted with the PCDH15 transmembrane domain (Fig. 3D). We conclude that the transmembrane and membrane proximal CR domain of PCDH15 mediate interaction with TMHS.

TMHS does not bind to CDH23, harmonin, and SANS (Fig. 3E) providing further evidence for a specific functional link between PCDH15 and TMHS.

TMHS regulates PCDH15 cell surface expression

Based on the interdependence of PCDH15 and TMHS for their efficient localization to stereocilia, we reasoned that interaction between the two proteins might regulate their effective cell surface transport. We therefore analyzed the subcellular distribution of PCDH15 and TMHS in heterologous cells. We chose RPMI-2650 cells for this purpose because they have a flat morphology with an extensive cytoplasm. In the absence of PCDH15, TMHS accumulated in clusters in the cytoplasm (Fig. 4Aa, B). Similarly, without TMHS, PCDH15 accumulated around the nucleus of transfected cells in rod-like aggregates (Fig. 4Ab, B). Few cells showed low levels of PCDH15 in cell protrusions (Fig. 4Ac, arrows; Fig. 4B) indicative of inefficient protein transport. The distribution of TMHS and PCDH15 were altered upon co-expression of the two proteins (Fig. 4Ad-f). One day after transfection, TMHS prominently co-localized with PCDH15 at the plasma membrane (Fig. 4Ad-f; Fig. 4B,C). Staining of non-permeabilized cells with an antibody to the extracellular PCDH15 domain confirmed that PCDH15 was localized at the cell surface upon co-expression with TMHS (Fig. 4Ae, insert). After 4 days in culture, PCDH15 and TMHS accumulated in the plasma membrane in a punctate pattern (Fig. 4Ag-i), indicating that the two proteins clustered into membrane microdomains. We conclude that PCDH15 and TMHS facilitate each other's cell surface transport.

TMHS mutations that cause deafness affect PCDH15 cell surface expression

TMHS mutations have been reported that cause hearing loss (Fig. 4C) (Longo-Guess et al., 2005; Longo-Guess et al., 2007; Shabbir et al., 2006). None of the mutations affected interactions between TMHS and PCDH15 as analyzed by co-immunoprecipitation experiments (Fig. 4D). When we co-expressed PCDH15 and TMHS carrying the *hurry-scurry* mutation in RPMI-2650 cells, PCDH15 and TMHS still co-localized (Fig. 4E), but the protein complex remained in aggregates within the cytoplasm, suggesting that some TMHS mutations cause deafness by affecting PCDH15 transport. Since we did not observe accumulation of PCDH15/TMHS in the cell bodies of hair cells in TMHS-/PCDH15-deficient mice (data not shown), defects in protein transport likely affect protein stability in vivo.

Expression of TMHS and PCDH15 in TMHS-deficient hair cells restores mechanotransduction

To exclude that general defects in hair cell development account for the mechanotransduction defect in OHCs from *Tmhs*$^{-/-}$ mice, we determined whether acute expression of TMHS in mutant hair cells rescues transduction. To facilitate the experiments, we developed an electroporation method for the expression of cDNAs in hair cells, combined with the analysis of mechanotransduction currents using the genetically encoded Ca^{2+} sensor G-CaMP3 (Tian et al., 2009). We confirmed by patch clamp physiology that the

electroporation method was compatible with measuring transduction currents (Supplementary Fig. S2). Next, we evaluated the feasibility to use G-CaMP3 as a read-out for mechanotransduction currents. We electroporated hair cells from wild-type mice at P4 with G-CaMP3, cultured them for 1 day (Fig. 5A), and activated transduction channels in OHCs with a fluid jet, by applying three sequential stimuli of increasing duration. Following stimulation, fluorescence intensity increased robustly in OHCs expressing G-CaMP3 (Fig. 5B). Little increase was observed in OHCs from *Tmhs*$^{-/-}$ mice (Fig. 5B), or in the presence of the transduction channel blocker dihydrostreptomycin (Fig. 5C). We conclude that the fluorescence signal is a useful readout for the activation of transduction channels, although changes in fluorescence intensity likely also depend on the activation of Ca^{2+} channels downstream of the transducer channel.

Previous studies have shown that the mechanotransduction machinery of cochlear hair cells matures in the first few postnatal days, where the amplitude of the transducer currents increases over time (Waguespack et al., 2007). Consistent with this finding, we observed that fluid-jet induced changes in Ca^{2+} fluorescence intensity were significantly higher in wild-type OHCs electroporated at P4 when compared to P1 (Fig. 5D). We could evoke minimal changes in Ca^{2+} fluorescence intensity in OHCs from *Tmhs*$^{-/-}$ mice transfected at either age (Fig. 5D).

Next, we determined the extent to which mechanotransduction in OHCs from *Tmhs*$^{-/-}$ mice is rescued by expression of TMHS. Expression of wild-type TMHS or TMHS carrying the *hurry-scurry* mutation did not affect mechanically evoked transducer currents in wild-type OHCs (Fig. 5E). However, wild-type but not mutant TMHS restored mechanical sensitivity in OHCs from *Tmhs*$^{-/-}$ mice transfected at P2 (Fig. 5E) or P5 (Fig. 5F). These data were confirmed by analyzing mechanically evoked transducer currents using whole cell recordings (Supplementary Fig. S2). We conclude that the transduction defect in *Tmhs*$^{-/-}$ mice is likely not a secondary consequence of defects in overall hair cell development.

Instead, our histochemical and biochemical data suggest that effects of TMHS mutations on mechanotransduction are caused by inefficient PCDH15 transport. If this is true, overexpression of PCDH15 in hair cells from *Tmhs*$^{-/-}$ mice might rescue transduction. To test this model, we generated a cDNA expression vector for PCDH15-CD3. As a control, we expressed PCDH15-CD3 in PCDH15-deficient OHCs from *Ames waltzer*$^{av3J/av3J}$ mice. Acute expression of PCDH15-CD3 rescued their mechanotransduction defect, demonstrating the effectiveness of our expression vector to restore PCDH15 function (Fig. 5G). Significantly, expression of PCDH15 in OHCs from *Tmhs*$^{-/-}$ mice also restored transduction (Fig. 5H). The data provide compelling evidence that transduction defects in *Tmhs*$^{-/-}$ mice are caused by defects in PCDH15 function, and support the model that PCDH15 can be transported to stereocilia in the absence of TMHS but only when expressed at high levels.

TMHS expression in OHCs from PCDH15-deficient *Ames waltzer*$^{av3J/av3J}$ mice did not restore transduction (Fig. 5I). This is not surprising since TMHS is not expected to restore tip links in the absence of the essential tip-link component PCDH15.

Macroscopic mechanotransduction currents

The γ subunits of Ca_v channels and the TARPs of AMPA receptors are required for efficient plasma membrane localization of their respective ion channels, but they also regulate ion channel pore properties (Dai et al., 2009; Jackson and Nicoll, 2011; Pongs and Schwarz, 2010; Vacher et al., 2008). We wondered whether TMHS might similarly affect the assembly of the hair cells mechanotransduction machinery and channel function. To test this

model, we analyzed the remaining mechanotransduction currents in OHCs from *Tmhs*$^{-/-}$ mice.

Hair bundles were stimulated with a stiff glass probe. As reported (Grillet et al., 2009b; Kennedy et al., 2003; Kros et al., 2002; Stauffer et al., 2005; Waguespack et al., 2007), control OHCs had rapidly activating transducer currents, which subsequently adapted with a fast and slow time constant (Fig. 6A). The amplitude of saturated mechanotransduction currents was at 540.9 ± 27.8pA. In hair cells from mutant mice, peak amplitudes reached 58.7 ± 5.9 pA (Fig. 6A,B), suggesting that the number of active mechanotransduction channels was reduced, which is consistent with the reduced number of tip links in *Tmhs*$^{-/-}$ OHCs. The shape of the current traces obtained from mutant OHCs were also altered and revealed an apparent lack of adaptation (Fig. 6A). To normalize for variations in amplitude, we plotted the open probability of the transducer channel (Po) against displacement (Fig. 6C). The resulting curve from mutants was significantly shifted to the right and broadened when compared to wild-type, indicative of less coordinated channel gating throughout the hair bundle and reduced sensitivity to deflection.

To analyze adaptation further, we applied a set of deflections ranging from -100 nm to 1000 nm to hair bundles. Each deflection lasted for 30 ms, after which adaptation is largely complete. To compare the kinetic properties of the mechanotransducer currents, we superimposed current traces from controls and mutants based on similar steady-state currents (Fig. 6D). The fast adaptation phase was no longer observable in OHCs from *Tmhs*$^{-/-}$ mice. To quantify the changes, we plotted the ratio of steady-state current to peak current (Rsteady-state/peak) versus the channels open probability (P_o) (Fig. 6E). The Rsteady-state/peak of the control increased from 0.36 ± 0.02 to 0.73 ± 0.02, while the Rsteady-state/peak of mutants ranged from 0.64 ± 0.06 to 0.80 ± 0.18, consistent with perturbed fast adaptation. Since current amplitudes in OHCs from mutant mice were small and peak currents were sometimes difficult to determine, we did not calculate the time-constant for fast adaptation.

The activation of transduction channels in OHCs from *Tmhs*$^{-/-}$ mice was also affected (Fig. 6D, inset). In control OHCs, the activation time constant ranged from 85 ± 3 μs to 97 ± 7 μs, which was within the rise time of our stimulus probe (Fig. 6F). In mutant OHCs, activation kinetics was significantly slower ranging from 252 ± 26 μs to 426 ± 150 μs (Fig. 6F). In wild-type a relative stable τ with increasing deflection was observed, which is in agreement with published findings for rat and mouse hair cells (Kennedy et al., 2003; Ricci et al., 2005). In mutant hair cells, we did not observe a change in τ with increasing deflections either and activation was significantly slowed down compared to controls (Fig. 6D). These changes in channel activation could be caused by alterations in the channel protein and/or in its environment such as in the stiffness of the membrane.

Analysis of the voltage dependence of transducer currents and its sensitivity to external Ca^{2+} did not reveal differences between hair cells from wild-type and mutant mice (Supplementary Fig. S3) indicating that the observed changes in the properties of the transducer currents in the absence of TMHS are not a consequence of alterations in the way external Ca^{2+} blocks the channel.

We conclude that fewer transduction channels are activated in mutant *Tmhs*$^{-/-}$ OHCs compared to wild-type, likely because tip link numbers are reduced in the mutants. We also observed variable onset of transducer currents, indicating that the function of the remaining tip-link complexes was altered directly or as a consequence of less coherent force propagation through the hair bundle. Moreover, adaptation appeared to be affected, which

could be a consequence of a reduction in the number of active channels, delay in channel activation, and less coordinated activation by remaining tip links.

Single channel properties

The effects of TMHS loss on macroscopic mechanotransduction currents could be caused by a reduction in the number of active channel complexes within a hair bundle. However, since TMHS binds to PCDH15, which is in close proximity to the transduction channel, we wondered whether TMHS might affect the channel directly. We carried out single channel recordings, taking advantage of the observation that tip links can be broken by Ca^{2+} removal, reducing the number of active transduction channels until single channel events can be recorded (Beurg et al., 2006; Ricci et al., 2003). We delivered with a fluid jet an EGTA solution to wild-type and mutant hair bundles at a similar position (40% of the distance along the cochlea from the low frequency end). Mechanotransduction channels were then activated with a Piezo stimulator and channel activity was recorded in the whole-cell configuration. Fig. 7A,B show typical single channel events obtained with a 300 nm deflection in controls (left panel) and mutants (right panel). Single channel events of a similar amplitude and duration as reported earlier (Beurg et al., 2006; Ricci et al., 2003) were observed in control OHCs. Transducer current ensemble averages from wild-type OHCs (Fig. 7A; left panel, middle) resembled macroscopic currents remarkably well, where transducer currents rapidly activated, followed by adaptation. In contrast, ensemble averages in *Tmhs*$^{-/-}$ OHCs (Fig. 7A; right panel, middle) lacked the adaptation phase. Amplitude histograms are shown to indicate open and close state of single channel events (Fig. 7A; bottom). Analysis of single channel events from current traces of a number of cells (see figure legend for numbers) established several differences in the behavior of single channels from *Tmhs*$^{-/-}$ OHCs: (i) the average conductance in controls was at 86.8±1.6 pS and in the mutants at 68.1±1.7 pS (Fig. 7C); (ii) the latency between the onset of deflection and the first channel event was longer in mutant OHCs (2.3 ms) compared to wild-type (1.3 ms) (Fig. 7D); (iii) the τ of the average open time of single event in mutant OHCs was ~1.7 fold increased compared to controls (Fig. 7B).

DISCUSSION

We provide here evidence that TMHS is intimately linked to the function of the hair cells mechanotransduction machinery. First, TMHS is localized at least in part to the tips of hair cell stereocilia in close proximity to their tip links. While TMHS mRNA is present in developing and adult hair cells, it is difficult to detect TMHS protein after P7. This is likely due to the limited sensitivity of our antibody. Second, TMHS binds to the transmembrane and CR domains of PCDH15, which is located in close proximity to the transduction channel. Third, TMHS is required for tip link integrity. Finally, transducer channel properties are altered in *Tmhs*$^{-/-}$ OHCs. We conclude that TMHS is associated with PCDH15 and the mechanotransduction channel and regulates the response of the transduction channel to mechanical stimulation (Fig. 7E).

Ion channels usually consist of pore forming and accessory proteins. Some ion channel subunits share with TMHS a 4 transmembrane topology. Examples include the pore forming subunits of the CRAC channel (Feske et al., 2006; Vig et al., 2006), the accessory γ-1 subunit of Ca_v channels (Jay et al., 1990), and the TARP subunits of AMPA receptors such as stargazin (Letts et al., 1998). Our findings suggest that TMHS is functionally similar to accessory ion channel subunits such as γ-1 or stargazin, which regulate ion channel transport and conductance (Dai et al., 2009; Jackson and Nicoll, 2011; Pongs and Schwarz, 2010; Vacher et al., 2008). In analogy, TMHS regulates conductance through the hair cell's mechanotransduction channel, is required for fast adaptation, and for efficient PCDH15 localization to stereocilia. In the absence of TMHS some tip links form, suggesting that

TMHS is not absolutely essential for PCDH15 transport. Consistent with this model, small amounts of PCDH15 are transported to the surface of transfected cells in the absence of TMHS. In hair cells, PCDH15 is expressed at high levels during development; its expression level decreases subsequently (Ahmed et al., 2006; Webb et al., 2011). Developing hair bundles may depend less on TMHS, which is consistent with the observation that TMHS-deficient hair bundles show less severe morphological defects than PCDH15-deficient hair bundles. While mechanotransduction currents can be elicited in *Tmhs*$^{-/-}$ stereocilia that contain tip links, channel activation is delayed, suggesting that coupling between the transduction channel and PCDH15 is less efficient. TMHS might stabilize interactions between PCDH15 and the channel, and/or it might affect membrane properties locally, which is a function attributed to some tetraspans (Yanez-Mo et al., 2009).

The current amplitude of the macroscopic transducer currents in *TMHS*$^{-/-}$ OHCs is reduced, which can be explained at least in part by the reduced numbers of tip links. Channel activation is slowed and adaptation is nearly absent. While some of these changes might be explained by less coordinated and delayed activation of fewer mechanotransduction channels, our single channel analysis demonstrates that in *Tmhs*$^{-/-}$ mice the properties of the transduction channel are altered. In the absence of TMHS, channel conductance is reduced by ~22%, indicating that TMHS affects the channel pore. Latency and open time of single channels in *TMHS*$^{-/-}$ OHCs are increased by ~70%, which is consistent with the increased activation time constant and lack of fast adaptation observed in macroscopic currents. The decreased amplitude of single channel currents, together with increased latency and channel open time, suggests that TMHS functionally couples the mechanotransduction channel to the tip link.

In analogy to γ-1 and TARP subunits, changes in the properties of the mechanotransduction channel in *Tmhs*$^{-/-}$ mice can perhaps be explained best by an allosteric mechanism, where TMHS binds to pore forming subunits of the mechanotransduction channel to affect the conformation of the channel complex. Changes in gating kinetics such as increased latency as well as adaptation defects can be explained by direct effects of TMHS on the channel, or by changes in the channels environment such as the stiffness of the membrane.

The conductance properties of the transduction channel in OHCs vary from the cochlear base to the apex, suggesting that the molecular composition of the channel varies (Ricci et al., 2003). Since TMHS regulates channel conductance, variations in TMHS expression could explain tonotopic differences in currents. Notably, TMHS is a member of a small tetraspan subfamily (Longo-Guess et al., 2005). While the expression pattern of TMHS homologous needs to be determined, this raises the possibility that different TMHS-like proteins might generate mechanotransduction channels with different properties. The pore forming subunits of the hair cells mechanotransduction channel still need to be identified, but some candidates have emerged including TMC-1,TMC-2 (Kawashima et al., 2011), Piezo1 and Piezo2 (Coste et al., 2010; Coste et al., 2012). It will be important to analyze functional interactions between TMHS and these proteins.

Finally, our findings are significant for understanding disease mechanisms. We establish an unanticipated link in the mechanism by which mutations in TMHS and PCDH15 cause hearing loss. Our findings suggest that at least in some patients with mutations in TMHS and PCDH15 deafness is caused by functional impairment of the hair cells mechanotransduction machinery.

EXPERIMENTAL PROCEDURES

Detailed experimental procedures are described in the supplement.

Mouse strains

Rumba, *samba*, *sirtaki*, *pogo*, *salsa*, *hurry-scurry*, TMHS knock-out, *harmonin PDZ2*, *Ames waltzer*^{av3j}, and *waltzer*^{v2j} mice have been described (Alagramam et al., 2001; Di Palma et al., 2001; Grillet et al., 2009a; Grillet et al., 2009b; Longo-Guess et al., 2005; Longo-Guess et al., 2007; Schwander et al., 2007; Schwander et al., 2009)

In situ hybridization, antibodies, whole mount staining and immunocytochemistry

In situ hybridizations and cochlear whole mount stainings were carried out as described (Senften et al., 2006). Primary antibodies were as follows: α-TMHS (Longo-Guess et al., 2005); α-CDH23 (Kazmierczak et al., 2007); α-PCDH15; (Kazmierczak et al., 2007); α-harmonin (Grillet et al., 2009b); a-HA (clone 6E2, Cell Signaling). Additional reagents were: Alexa Fluor 488-phalloidin, Alexa Fluor 594 goat anti-rabbit, TOP-RO3 and Alexa Fluor 647-phalloidin (Invitrogen, Carlsbad, CA).

Scanning electron microscopy

Inner ears were dissected and fixed. The stria vascularis, Reissner's membrane and tectorial membrane were removed. Samples were dehydrated, processed to critical drying point, mounted, coated with iridium and imaged. Quantification of hair bundle morphology and tip links was carried out as described in the supplement.

DNA constructs, transfections, immunoprecipitations and Western blots

DNA constructs are described in Supplementary Information. Expression of the constructs, immunoprecipitations, and Western blots were carried out as described (Senften et al., 2006). Immunoprecipitation experiments were carried out at least 3 times.

Cochlea culture and electroporation

The organ of Corti was dissected from P0-8 mice as described (Grillet et al., 2009b) and cut into 3 pieces, which were placed in DMEM/F12 medium with 10% FBS and 1.5 μg/ml ampicillin. For electroporation, glass electrodes (2 μm diameter) were used to deliver plasmid (1 μg/μl in 1x HBSS) to the sensory epithelium. For Ca^{2+} imaging, we used G-CaMP3 (Addgene 22692). A series of 3 pulses was applied at 1 sec intervals with a magnitude of 60V and duration of 15 msec (ECM 830 square wave electroporator; BTX). Hair cells were imaged on an upright Olympus BX51WI microscope. Hair bundles were stimulated with a fluid jet applied through a glass electrode filled with bath solution.

Stimuli were applied using Patchmaster 2.35 software (HEKA) and 20 psi air pressure. Images were collected with a 2 sec sampling rate. A series of fluid-jet stimulations (0.1, 0.3, 0.5 sec) was applied (80 sec intervals). Responses induced by 0.3 sec fluid-jet stimulation were used for quantitative analysis.

Electrophysiology

For recording, tissue was transferred to the recording chamber and a peristaltic pump was used to perfuse artificial perilymph. Hair bundles were deflected with a glass pipette mounted on a P-885 piezoelectric stack actuator (Physik Instrument). The actuator was driven with voltage steps that were low-pass filtered at 10 KHz. Whole cell recording were carried out and currents were sampled at 100 KHz. Macroscopic currents were recorded essentially as we have described (Grillet et al., 2009b). For single channel recordings, we followed published procedures (Ricci et al., 2003).

Data analysis

Data analysis was performed using Excel (Microsoft) and Igor pro 6 (WaveMetrics, Lake Oswego, OR). Calcium signal ($\Delta F/F$) was calculated with the equation: $(F-F_0)/F_0$, where F_0 is the averaged fluorescence baseline at the beginning. Transduction current-displacement curves (I(X)) were fitted with a three-state Boltzmann model to calculate channel open probability (P_o) as described (Grillet et al., 2009b). All data are mean ± SEM. Student's two-tailed unpaired t test was used to determine statistical significance (*, $p<0.05$, **, $p<0.01$, ***, $p<0.001$).

Supplementary Material

Refer to Web version on PubMed Central for supplementary material.

Acknowledgments

W.X carried out the electrophysiological recordings, calcium imaging experiments, and the analysis of protein localization in tranfected cells. W.X. and T.W. developed the electroporation technique. N.G. carried out in situ hybridizations and the analysis of hair cell morphology and tip links by SEM. W.X, N.G., T.W., and P.K. carried out immunolocalization experiments in hair cells. H.E. and B.Z. generated plasmid constructs and carried out co-immunoprecipitation experiments. K.J. provided TMHS mutant mice and generated the TMHS antibody. W.X., N.G., T.W., P.K. and U.M. contributed to the planning of the work. U.M. wrote the manuscript with help from W.X. and N.G.. We thank S.W. Webb and S.R. Harkins-Perry for cloning constructs. This work was supported by the NIH (U.M. DC005965, DC007704), the Dorris Neuroscience Center, the Skaggs Institute for Chemical Biology, and the Bundy Foundation (W.X. and U.M.).

REFERENCES

Adato A, Michel V, Kikkawa Y, Reiners J, Alagramam KN, Weil D, Yonekawa H, Wolfrum U, El-Amraoui A, Petit C. Interactions in the network of Usher syndrome type 1 proteins. Hum Mol Genet. 2005; 14:347–356. [PubMed: 15590703]

Ahmed ZM, Goodyear R, Riazuddin S, Lagziel A, Legan PK, Behra M, Burgess SM, Lilley KS, Wilcox ER, Riazuddin S, et al. The tip-link antigen, a protein associated with the transduction complex of sensory hair cells, is protocadherin-15. J Neurosci. 2006; 26:7022–7034. [PubMed: 16807332]

Alagramam KN, Murcia CL, Kwon HY, Pawlowski KS, Wright CG, Woychik RP. The mouse Ames waltzer hearing-loss mutant is caused by mutation of Pcdh15, a novel protocadherin gene. Nat Genet. 2001; 27:99–102. [PubMed: 11138007]

Bahloul A, Michel V, Hardelin JP, Nouaille S, Hoos S, Houdusse A, England P, Petit C. Cadherin-23, myosin VIIa and harmonin, encoded by Usher syndrome type I genes, form a ternary complex and interact with membrane phospholipids. Hum Mol Genet. 2010; 19:3557–3565. [PubMed: 20639393]

Beurg M, Evans MG, Hackney CM, Fettiplace R. A large-conductance calcium-selective mechanotransducer channel in mammalian cochlear hair cells. J Neurosci. 2006; 26:10992–11000. [PubMed: 17065441]

Beurg M, Fettiplace R, Nam JH, Ricci AJ. Localization of inner hair cell mechanotransducer channels using high-speed calcium imaging. Nat Neurosci. 2009

Boeda B, El-Amraoui A, Bahloul A, Goodyear R, Daviet L, Blanchard S, Perfettini I, Fath KR, Shorte S, Reiners J, et al. Myosin VIIa, harmonin and cadherin 23, three Usher I gene products that cooperate to shape the sensory hair cell bundle. Embo J. 2002; 21:6689–6699. [PubMed: 12485990]

Caberlotto E, Michel V, Foucher I, Bahloul A, Goodyear RJ, Pepermans E, Michalski N, Perfettini I, Alegria-Prevot O, Chardenoux S, et al. Usher type 1G protein sans is a critical component of the tip-link complex, a structure controlling actin polymerization in stereocilia. Proc Natl Acad Sci U S A. 2011; 108:5825–5830. [PubMed: 21436032]

Coste B, Mathur J, Schmidt M, Earley TJ, Ranade S, Petrus MJ, Dubin AE, Patapoutian A. Piezo1 and Piezo2 are essential components of distinct mechanically activated cation channels. Science. 2010; 330:55–60. [PubMed: 20813920]

Coste B, Xiao B, Santos JS, Syeda R, Grandl J, Spencer KS, Kim SE, Schmidt M, Mathur J, Dubin AE, et al. Piezo proteins are pore-forming subunits of mechanically activated channels. Nature. 2012; 483:176–181. [PubMed: 22343900]

Dai S, Hall DD, Hell JW. Supramolecular assemblies and localized regulation of voltage-gated ion channels. Physiol Rev. 2009; 89:411–452. [PubMed: 19342611]

Di Palma F, Holme RH, Bryda EC, Belyantseva IA, Pellegrino R, Kachar B, Steel KP, Noben-Trauth K. Mutations in Cdh23, encoding a new type of cadherin, cause stereocilia disorganization in waltzer, the mouse model for Usher syndrome type 1D. Nat Genet. 2001; 27:103–107. [PubMed: 11138008]

Feske S, Gwack Y, Prakriya M, Srikanth S, Puppel SH, Tanasa B, Hogan PG, Lewis RS, Daly M, Rao A. A mutation in Orai1 causes immune deficiency by abrogating CRAC channel function. Nature. 2006; 441:179–185. [PubMed: 16582901]

Gillespie PG, Muller U. Mechanotransduction by hair cells: models, molecules, and mechanisms. Cell. 2009; 139:33–44. [PubMed: 19804752]

Goodyear RJ, Marcotti W, Kros CJ, Richardson GP. Development and properties of stereociliary link types in hair cells of the mouse cochlea. J Comp Neurol. 2005; 485:75–85. [PubMed: 15776440]

Grati M, Kachar B. Myosin VIIa and sans localization at stereocilia upper tip-link density implicates these Usher syndrome proteins in mechanotransduction. Proc Natl Acad Sci U S A. 2011; 108:11476–11481. [PubMed: 21709241]

Grillet N, Schwander M, Hildebrand MS, Sczaniecka A, Kolatkar A, Velasco J, Webster JA, Kahrizi K, Najmabadi H, Kimberling WJ, et al. Mutations in LOXHD1, an evolutionarily conserved stereociliary protein, disrupt hair cell function in mice and cause progressive hearing loss in humans. Am J Hum Genet. 2009a; 85:328–337. [PubMed: 19732867]

Grillet N, Xiong W, Reynolds A, Kazmierczak P, Sato T, Lillo C, Dumont RA, Hintermann E, Sczaniecka A, Schwander M, et al. Harmonin mutations cause mechanotransduction defects in cochlear hair cells. Neuron. 2009b; 62:375–387. [PubMed: 19447093]

Holt JR, Gillespie SK, Provance DW, Shah K, Shokat KM, Corey DP, Mercer JA, Gillespie PG. A chemical-genetic strategy implicates myosin-1c in adaptation by hair cells. Cell. 2002; 108:371–381. [PubMed: 11853671]

Jackson AC, Nicoll RA. The expanding social network of ionotropic glutamate receptors: TARPs and other transmembrane auxiliary subunits. Neuron. 2011; 70:178–199. [PubMed: 21521608]

Jay SD, Ellis SB, McCue AF, Williams ME, Vedvick TS, Harpold MM, Campbell KP. Primary structure of the gamma subunit of the DHP-sensitive calcium channel from skeletal muscle. Science. 1990; 248:490–492. [PubMed: 2158672]

Kawashima Y, Geleoc GS, Kurima K, Labay V, Lelli A, Asai Y, Makishima T, Wu DK, Della Santina CC, Holt JR, et al. Mechanotransduction in mouse inner ear hair cells requires transmembrane channel-like genes. J Clin Invest. 2011; 121:4796–4809. [PubMed: 22105175]

Kazmierczak P, Sakaguchi H, Tokita J, Wilson-Kubalek EM, Milligan RA, Muller U, Kachar B. Cadherin 23 and protocadherin 15 interact to form tip-link filaments in sensory hair cells. Nature. 2007; 449:87–91. [PubMed: 17805295]

Kennedy HJ, Evans MG, Crawford AC, Fettiplace R. Fast adaptation of mechanoelectrical transducer channels in mammalian cochlear hair cells. Nat Neurosci. 2003; 6:832–836. [PubMed: 12872124]

Kros CJ, Marcotti W, van Netten SM, Self TJ, Libby RT, Brown SD, Richardson GP, Steel KP. Reduced climbing and increased slipping adaptation in cochlear hair cells of mice with Myo7a mutations. Nat Neurosci. 2002; 5:41–47. [PubMed: 11753415]

Lagziel A, Ahmed ZM, Schultz JM, Morell RJ, Belyantseva IA, Friedman TB. Spatiotemporal pattern and isoforms of cadherin 23 in wild type and waltzer mice during inner ear hair cell development. Dev Biol. 2005; 280:295–306. [PubMed: 15882574]

Lefevre G, Michel V, Weil D, Lepelletier L, Bizard E, Wolfrum U, Hardelin JP, Petit C. A core cochlear phenotype in USH1 mouse mutants implicates fibrous links of the hair bundle in its

cohesion, orientation and differential growth. Development. 2008; 135:1427–1437. [PubMed: 18339676]

Letts VA, Felix R, Biddlecome GH, Arikkath J, Mahaffey CL, Valenzuela A, Bartlett FS 2nd, Mori Y, Campbell KP, Frankel WN. The mouse stargazer gene encodes a neuronal Ca2+-channel gamma subunit. Nat Genet. 1998; 19:340–347. [PubMed: 9697694]

Longo-Guess CM, Gagnon LH, Cook SA, Wu J, Zheng QY, Johnson KR. A missense mutation in the previously undescribed gene Tmhs underlies deafness in hurry-scurry (hscy) mice. Proc Natl Acad Sci U S A. 2005; 102:7894–7899. [PubMed: 15905332]

Longo-Guess CM, Gagnon LH, Fritzsch B, Johnson KR. Targeted knockout and lacZ reporter expression of the mouse Tmhs deafness gene and characterization of the hscy-2J mutation. Mamm Genome. 2007; 18:646–656. [PubMed: 17876667]

McHugh RK, Friedman RA. Genetics of hearing loss: Allelism and modifier genes produce a phenotypic continuum. Anat Rec A Discov Mol Cell Evol Biol. 2006; 288:370–381. [PubMed: 16550584]

Michalski N, Michel V, Caberlotto E, Lefevre GM, van Aken AF, Tinevez JY, Bizard E, Houbron C, Weil D, Hardelin JP, et al. Harmonin-b, an actin-binding scaffold protein, is involved in the adaptation of mechanoelectrical transduction by sensory hair cells. Pflugers Arch. 2009; 459:115–130. [PubMed: 19756723]

Michel V, Goodyear RJ, Weil D, Marcotti W, Perfettini I, Wolfrum U, Kros CJ, Richardson GP, Petit C. Cadherin 23 is a component of the transient lateral links in the developing hair bundles of cochlear sensory cells. Dev Biol. 2005; 280:281–294. [PubMed: 15882573]

Pongs O, Schwarz JR. Ancillary subunits associated with voltage-dependent K+ channels. Physiol Rev. 2010; 90:755–796. [PubMed: 20393197]

Ricci AJ, Crawford AC, Fettiplace R. Tonotopic variation in the conductance of the hair cell mechanotransducer channel. Neuron. 2003; 40:983–990. [PubMed: 14659096]

Ricci AJ, Kennedy HJ, Crawford AC, Fettiplace R. The transduction channel filter in auditory hair cells. J Neurosci. 2005; 25:7831–7839. [PubMed: 16120785]

Sakaguchi H, Tokita J, Muller U, Kachar B. Tip links in hair cells: molecular composition and role in hearing loss. Curr Opin Otolaryngol Head Neck Surg. 2009; 17:388–393. [PubMed: 19633555]

Schwander M, Sczaniecka A, Grillet N, Bailey JS, Avenarius M, Najmabadi H, Steffy BM, Federe GC, Lagler EA, Banan R, et al. A forward genetics screen in mice identifies recessive deafness traits and reveals that pejvakin is essential for outer hair cell function. J Neurosci. 2007; 27:2163–2175. [PubMed: 17329413]

Schwander M, Xiong W, Tokita J, Lelli A, Elledge HM, Kazmierczak P, Sczaniecka A, Kolatkar A, Wiltshire T, Kuhn P, et al. A mouse model for nonsyndromic deafness (DFNB12) links hearing loss to defects in tip links of mechanosensory hair cells. Proc Natl Acad Sci U S A. 2009

Senften M, Schwander M, Kazmierczak P, Lillo C, Shin JB, Hasson T, Geleoc GS, Gillespie PG, Williams D, Holt JR, et al. Physical and functional interaction between protocadherin 15 and myosin VIIa in mechanosensory hair cells. J Neurosci. 2006; 26:2060–2071. [PubMed: 16481439]

Shabbir MI, Ahmed ZM, Khan SY, Riazuddin S, Waryah AM, Khan SN, Camps RD, Ghosh M, Kabra M, Belyantseva IA, et al. Mutations of human TMHS cause recessively inherited non-syndromic hearing loss. Journal of medical genetics. 2006; 43:634–640. [PubMed: 16459341]

Siemens J, Kazmierczak P, Reynolds A, Sticker M, Littlewood-Evans A, Muller U. The Usher syndrome proteins cadherin 23 and harmonin form a complex by means of PDZ-domain interactions. Proc Natl Acad Sci U S A. 2002; 99:14946–14951. [PubMed: 12407180]

Siemens J, Lillo C, Dumont RA, Reynolds A, Williams DS, Gillespie PG, Muller U. Cadherin 23 is a component of the tip link in hair-cell stereocilia. Nature. 2004; 428:950–955. [PubMed: 15057245]

Sollner C, Rauch GJ, Siemens J, Geisler R, Schuster SC, Muller U, Nicolson T. Mutations in cadherin 23 affect tip links in zebrafish sensory hair cells. Nature. 2004; 428:955–959. [PubMed: 15057246]

Stauffer EA, Scarborough JD, Hirono M, Miller ED, Shah K, Mercer JA, Holt JR, Gillespie PG. Fast adaptation in vestibular hair cells requires Myosin-1c activity. Neuron. 2005; 47:541–553. [PubMed: 16102537]

Tian L, Hires SA, Mao T, Huber D, Chiappe ME, Chalasani SH, Petreanu L, Akerboom J, McKinney SA, Schreiter ER, et al. Imaging neural activity in worms, flies and mice with improved GCaMP calcium indicators. Nat Methods. 2009; 6:875–881. [PubMed: 19898485]

Vacher H, Mohapatra DP, Trimmer JS. Localization and targeting of voltage-dependent ion channels in mammalian central neurons. Physiol Rev. 2008; 88:1407–1447. [PubMed: 18923186]

Vig M, Peinelt C, Beck A, Koomoa DL, Rabah D, Koblan-Huberson M, Kraft S, Turner H, Fleig A, Penner R, et al. CRACM1 is a plasma membrane protein essential for store-operated Ca2+ entry. Science. 2006; 312:1220–1223. [PubMed: 16645049]

Waguespack J, Salles FT, Kachar B, Ricci AJ. Stepwise morphological and functional maturation of mechanotransduction in rat outer hair cells. J Neurosci. 2007; 27:13890–13902. [PubMed: 18077701]

Webb SW, Grillet N, Andrade LR, Xiong W, Swarthout L, Della Santina CC, Kachar B, Muller U. Regulation of PCDH15 function in mechanosensory hair cells by alternative splicing of the cytoplasmic domain. Development. 2011; 138:1607–1617. [PubMed: 21427143]

Wilson SM, Householder DB, Coppola V, Tessarollo L, Fritzsch B, Lee EC, Goss D, Carlson GA, Copeland NG, Jenkins NA. Mutations in Cdh23 cause nonsyndromic hearing loss in waltzer mice. Genomics. 2001; 74:228–233. [PubMed: 11386759]

Yanez-Mo M, Barreiro O, Gordon-Alonso M, Sala-Valdes M, Sanchez-Madrid F. Tetraspanin-enriched microdomains: a functional unit in cell plasma membranes. Trends Cell Biol. 2009; 19:434–446. [PubMed: 19709882]

HIGHLIGHTS

- TMHS is a component of the hair cells mechanotransduction machinery
- TMHS binds to the tip-link component PCDH15 and regulates tip-link assembly
- TMHS regulates transducer channel conductance and is required for adaptation
- TMHS is structurally similar to other ion channel regulatory subunits such as TARPs

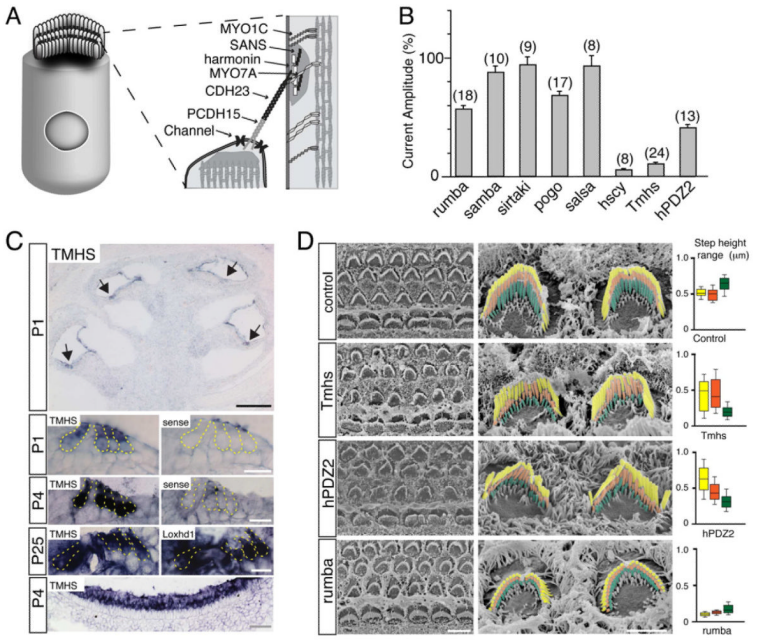

Figure 1. Mechanotransduction defects in TMHS-deficient mice

(A) Hair cell diagram showing on the right proteins that form tip links or are located in proximity to tip links. (B) Amplitude of mechanotransduction currents in mutant mouse lines. The values are expressed relative to the values in wild-type. The number of hair cells analyzed is indicated. Values are mean ± SEM. (C) In situ hybridization with TMHS antisense, sense control probes, and a Loxhd1 probe that reveals hair cells. The lowest panel shows vestibular hair cells, the magnified images hair cells at the apical-medial turn of the cochlea. Arrows point to hair cells. (D) SEM analysis of hair bundles from the mid-apical cochlea. On the right, OHCs are shown. The different rows of stereocilia have been colored. Whisker plots on the right show height differences between the first (longest) and second row of stereocilia (yellow); the second and third row (orange); the third row and surface of hair cells or lowest row (green) (number of evaluated hair bundles: control, n=16; *Tmhs*$^{-/-}$, n=21; hPDZ, n=21; *rumba*, n=12; from 2 animals each). Scale bars: (C) black bar: 200 μm; white bar, 50 μm; gray bar, 20 μm; (D) left panel: 5 μm; right panel 2 μm. See also Figure S1.

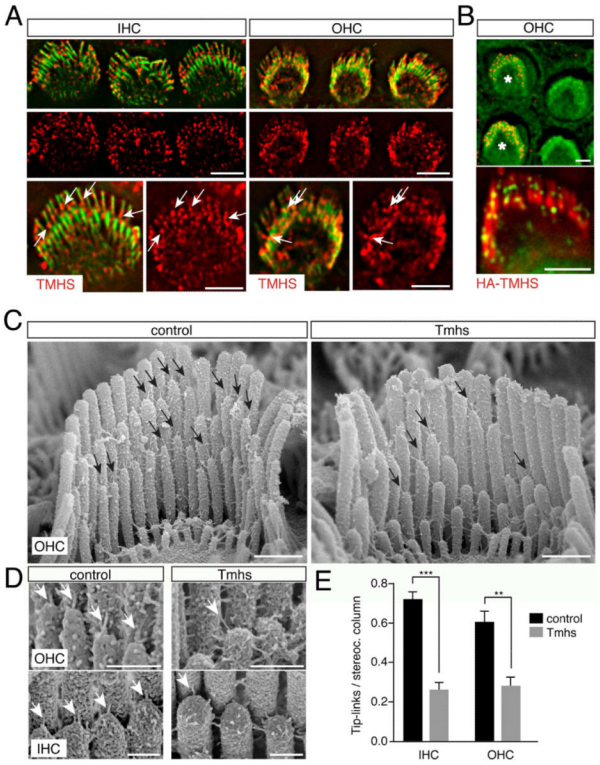

Figure 2. Tip-link defects in hair cells from TMHS$^{-/-}$ mice

(A) Hair cells from wild-type mice at P5 were stained with antibodies to TMHS (red) and with phalloidin (green). Arrows point to TMHS in the tip-link region. (B) OHCs were electroporated to express HA-TMHS (electroporated cells labeled with an asterisk). Cells were stained for HA (red in upper panel, green in lower panel) and with phalloidin (green in upper panel, red in lower panel). (C) SEM analysis of OHCs at P7. Arrows point to tip links. (D) High resolution images showing tip links (arrows) in OHCs and IHCs. (E) Quantification of tip-link numbers at P7. Values are mean ± SD (**, $p<0.01$; ***, $p<0.001$). Scale bar: (A, B) 3 μm; (C) 0.5 μm; (D) 0.25 μm.

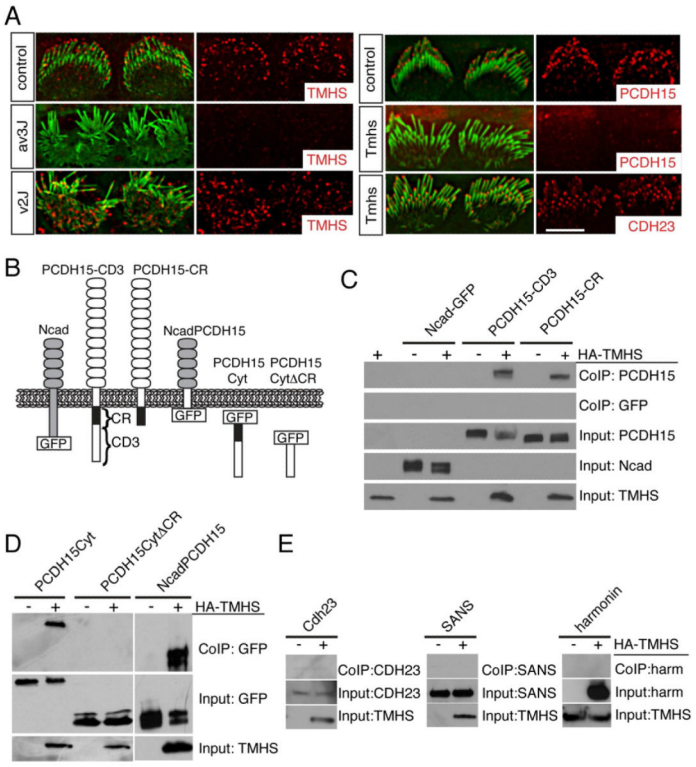

Figure 3. Interactions between TMHS and PCDH15

(A) IHCs from P1 wild-type mice, PCDH15 deficient *Ames waltzer*$^{av3J/av3J}$ mice, CDH23 deficient *waltzer*$^{v2J/v2J}$ mice, and *Tmhs*$^{-/-}$ mice were stained with antibodies to TMHS, PCDH15 and CDH23 (red) and phalloidin (green). Note the reduced staining of TMHS in PCDH15-muants and of PCDH15 in TMHS mutants. (B) Diagram of the constructs used for biochemical experiments. (C-E) HEK293 cells were transfected with the constructs indicated on top of each panel. Immunoprecipitations were carried out with HA antibodies that recognize HA-TMHS, followed by western blotting to detect PCDH15 constructs (C, D), CDH23, SANS, and harmonin (E). GFP-tagged PCDH15 and N-cadherin proteins were detected with an antibody to GFP, the remaining proteins with antibodies specific to the individual proteins. The lower rows show input protein, the upper rows co-immunoprecipitation (Co-IP) results. Note the specific interaction between TMHS and PCDH15. Scale bars: (A) 4 μm.

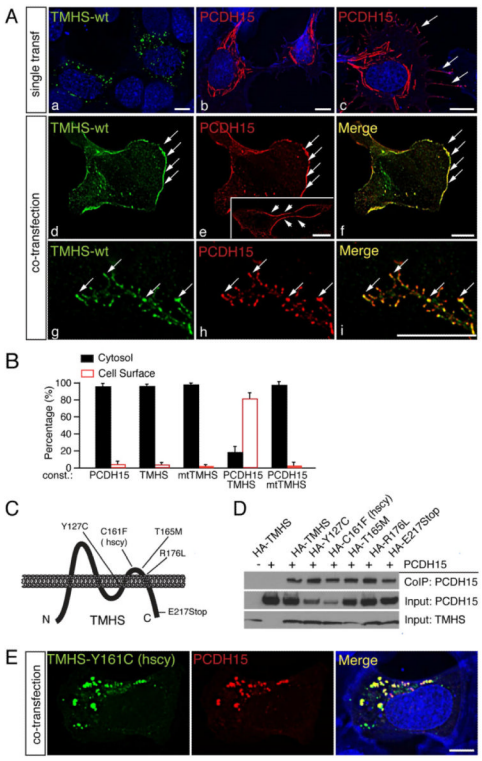

Figure 4. Wild-type but not mutant TMHS facilitates PCDH15 transport to the plasma membrane

(A) RPMI-2650 cells were transfected with expression vectors for TMHS and/or PCDH15 and analyzed for protein expression and localization one day after transfection (a-f) or four days after transfection (g-i). TMHS is shown in green, PCDH15 in red. Nuclei (a-c, blue) and actin (b and c, blue) were stained with DAPI and phalloidin, respectively. Note the low levels of PCDH15 at the cell surface in the absence of TMHS (c, arrows), and extensive co-localization of PCDH15 and TMHS at the surface of double-transfected cells (d-f, arrows). The insert in panel e show staining of non-permeabilized cells with an antibody to the PCDH15 extracellular domain. Panels g-i show co-localization of TMHS and PCDH15 in small aggregates in cell protrusions (arrows) after four days in culture. (B) Quantification of expression of proteins in the cytosol/at the plasma membrane in RPMI-2650 cells transfected to express TMHS and/or PCDH15 (at least 100 cells were quantified in 3 independent experiments). Values are mean ± SEM. (C) Diagram of TMHS and location of mutations within the protein. (D) Co-immunoprecipitation experiments were carried out with extracts from transfected HEK293 cells. Transfected constructs are indicated on top. The lower rows show input protein, the upper rows co-immunoprecipitation (Co-IP) results. (E) RPMI-2650 cells were co-transfected with expression vectors for PCDH15 and TMHS carrying the *hurry-scurry* mutation. TMHS is in green, PCDH15 in red, and nuclei and actin in blue. Scale bars: (A) 7 μm; (B) 5 μm.

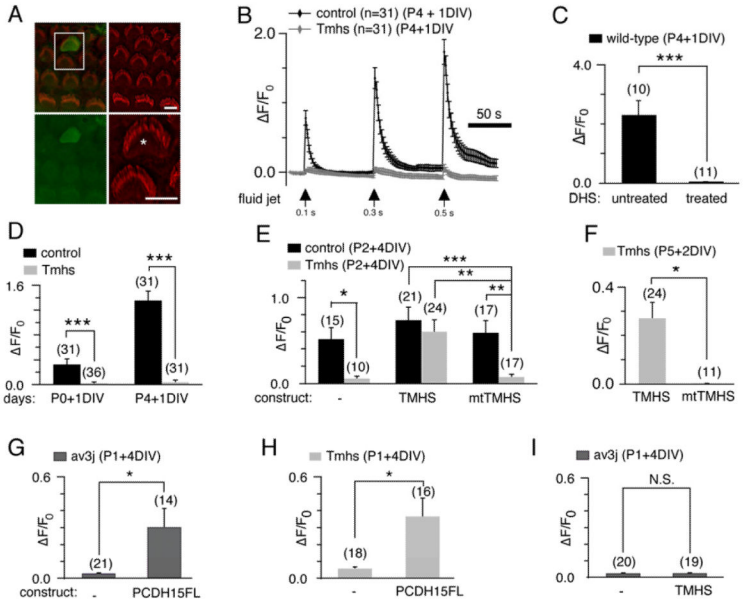

Figure 5. Rescue of mechanotransduction in *Tmhs*$^{-/-}$ mice by acute expression of TMHS and PCDH15

(A) Example of G-CaMP3 expression (green) in transfected OHC. Hair bundles of transfected cells are morphologically intact (Phalloidin staining, red), which can be seen in detail (asterisk) in the bottom-right panel. (B) Representative example demonstrating fluid-jet induced Ca^{2+} response in control and *Tmhs*$^{-/-}$ OHCs. OHCs were transfected at P4 and cultured for 1 day in vitro (DIV). Fluid-jet pulse duration was increased from 0.1 sec, to 0.3 sec, to 0.5 sec. For quantitative analysis (panels C-I), the amplitude of the 2nd Ca^{2+} response peak was measured. (C) Ca^{2+} response of wild type OHCs with/without dihydrostreptomycin (DHS). (D) Quantification of peak amplitude in OHCs from control and *Tmhs*$^{-/-}$ mice transfected at P0 or P4 and cultured for 1 DIV. (E) Response of OHCs from control and *Tmhs*$^{-/-}$ mice transfected to express G-CaMP3 only (-), wild-type TMHS (TMHS), or TMHS carrying the *hurry-scurry* mutation (mtTMHS). (F) OHCs from *Tmhs*$^{-/-}$ mice at P5 were transfected with wild-type and mutant TMHS and analyzed after 2 DIV for mechanically evoked Ca^{2+} currents. (G) Ca^{2+} responses in OHCs from PCDH15-deficient *Ames-waltzer*$^{av3J/av3J}$ mice electroporated to express PCDH15-CD3. (H) Ca^{2+} responses in OHCs from *Tmhs*$^{-/-}$ mice electroporated to express PCDH15-CD3. (I) Ca^{2+} responses in OHCs from PCDH15-deficient *Ames-waltzer*$^{av3J/av3J}$ mice electroporated to express TMHS. Please note that the changes in fluorescence intensity vary in magnitude between panels since we used for the experiments hair cells of different ages. All values are mean ± SEM (*, $p<0.05$; **, $p<0.01$; ***, $p<0.001$). Scale bars: (A) 6 μm. See also Figure S2.

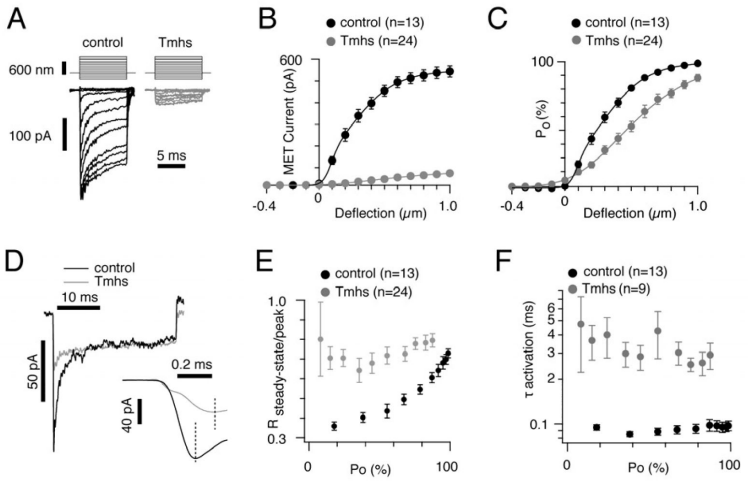

Figure 6. Macroscopic mechanotransduction currents in OHCs from *Tmhs*$^{-/-}$ mice

(A) Examples of transduction currents in OHCs from wild-type and *Tmhs*$^{-/-}$ mice in response to a set of 10 msec hair bundle deflections ranging from -400 nm to 1000 nm (100 nm steps). (B) Current displacement plots obtained from similar data as shown in (A). The number of analyzed hair cells is indicated. (C) Open probability (P_o) displacement plots calculated from similar data as shown in (A). The number of analyzed hair cells is indicated. (D) Representative current traces to show adaptation in OHCs from control and *Tmhs*$^{-/-}$ mice. Traces were chosen from controls and mutants based on similar steady state currents and similar rate of slow adaptation. Deflection was for 30 msec. Inset showed magnified traces for the activation phase of mechanically induced currents. (E) Ratio of steady-state current versus peak current plotted against the channel open probability (P_o). (F) Activation time constant (τactivation) plotted against P_o. All values are mean ± SEM (*, $p<0.05$; **, $p<0.01$; ***, $p<0.001$). See also Figure S3.

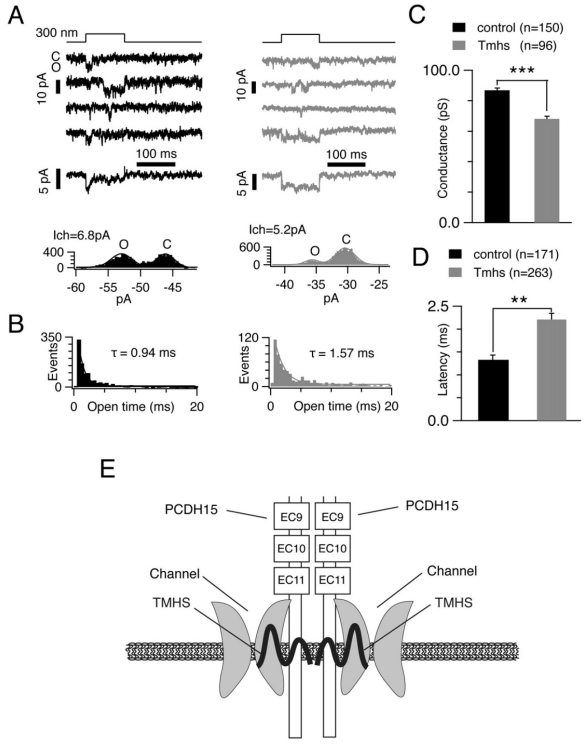

Figure 7. Single channel responses in OHCs from *Tmhs*$^{-/-}$ mice

(A) Upper panels: representative single channel recordings from a control (black) and *Tmhs*$^{-/-}$ (grey) OHC. Close (C) and open state (O) induced by a 300 nm deflection are shown. Middle panels: ensemble averages from 25 responses in controls and from 52 responses in mutants. The adaptation phase was only evident in ensemble averages from control OHC. Bottom panels: amplitude histograms generated with the data from the second traces in upper panels. Gaussian fits of the 2 peaks in the histograms determine a single channel conductance of 6.8 pA in control OHC and 5.2 pA in *Tmhs*$^{-/-}$ OHC. (B) Open-time histograms of single channel events from all recorded cells (control: 1691 events from 24 cells; mutant: 1663 events from 18 cells). The histograms were fitted with exponential curves with time constants of 0.94 ms in control (black) OHCs and 1.57 ms in *Tmhs*$^{-/-}$ (grey) OHCs. The first bin was not included for fitting as described (Ricci et al., 2003). (C) Amplitude of single channel currents from all recorded OHCs. Single channel conductance in OHCs from controls were at 86.8 ± 1.6 pS, and at 68.1 ± 1.7pS in OHCs from *Tmhs*$^{-/-}$ mice (controls: 150 traces from 19 cells; mutants: 96 traces from 8 cells). (D) Latency between the onset of deflection and first event from all recorded OHCs. Latency was at 1.3 ± 0.1 msec in control OHCs and at 2.2 ± 0.1 msec in *Tmhs*$^{-/-}$ OHCs (controls: 171 traces from 5 cells; mutants: 263 traces from 10 cells). All values are mean ± SEM (*, $p<0.05$; **, $p<0.01$; ***, $p<0.001$). (E) Model of the function of TMHS in hair cells. According to the model, TMHS is a regulatory subunit of the mechanotransduction channel that connects the pore forming subunits of the channel to PCDH15 and might also affect membrane properties.